



Natural killer cells migrate into and control simian immunodeficiency virus replication in lymph node follicles in African green monkeys

Nicolas Huot, Béatrice Jacquelin, Thalía Garcia-Tellez, Philippe Rascle, Mickaël Ploquin, Yoann Madec, R Keith Keith Reeves, Nathalie Derreudre-Bosquet, Michaela Müller-Trutwin

► To cite this version:

Nicolas Huot, Béatrice Jacquelin, Thalía Garcia-Tellez, Philippe Rascle, Mickaël Ploquin, et al.. Natural killer cells migrate into and control simian immunodeficiency virus replication in lymph node follicles in African green monkeys. *Nature Medicine*, 2017, 23 (11), pp.1277-1286. 10.1038/nm.4421 . pasteur-01984650

HAL Id: pasteur-01984650

<https://pasteur.hal.science/pasteur-01984650>

Submitted on 17 Jan 2019

HAL is a multi-disciplinary open access archive for the deposit and dissemination of scientific research documents, whether they are published or not. The documents may come from teaching and research institutions in France or abroad, or from public or private research centers.

L'archive ouverte pluridisciplinaire **HAL**, est destinée au dépôt et à la diffusion de documents scientifiques de niveau recherche, publiés ou non, émanant des établissements d'enseignement et de recherche français ou étrangers, des laboratoires publics ou privés.



Distributed under a Creative Commons Attribution - NonCommercial - ShareAlike 4.0 International License

1 NK cells migrate into and control SIV replication in lymph node
2 follicles in African green monkeys

3
4
5
6 Nicolas Huot^{1,2}, Beatrice Jacquelin¹, Thalia Garcia-Tellez¹, Philippe Rascle^{1,2,3},
7 Mickaël J Ploquin¹, Yoann Madec⁴, R Keith Reeves⁵, Nathalie Derreudre-Bosquet⁶
8 & Michaela Müller-Trutwin^{1,2}

9
10 ¹Institut Pasteur, HIV, Inflammation and Persistence Unit, Paris, France; ²Vaccine
11 Research Institute, Créteil, France; ³Université Paris Diderot, Sorbonne Paris Cité, Paris,
12 France ; ⁴Institut Pasteur, Epidemiology Unit, Paris, France; ⁵Center for Virology and
13 Vaccine Research, BIDMC, Harvard Medical School, Boston, MA, USA; ⁶CEA-
14 Université Paris Sud 11 INSERM U1184, Immunology of Viral Infections and
15 Autoimmune Diseases (IMVA), IBJF, IDMIT Department, Fontenay-aux-Roses, France.

16
17
18 **Keywords:** NK cells, SIV, HIV, non human primates, IL-15, CXCR5, lymph node,
19 spleen, B cell follicles, natural hosts, viral reservoir

20
21
22
23 **Corresponding author:** Michaela Müller-Trutwin
24 Institut Pasteur
25 HIV, Inflammation and Persistence Unit
26 28 rue du Dr Roux
27 75015 Paris, France
28 mmuller@pasteur.fr
29

30 **Abstract**

31

32 Natural Killer (NK) cells play an essential role in anti-viral immunity, but knowledge of their
33 function in secondary lymphoid organs is incomplete. Lymph node follicles constitute a major
34 viral reservoir during HIV-1 and SIVmac infections. In contrast, during non-pathogenic SIVagm
35 infection of African green monkeys (AGM), follicles remain generally virus-free. We show that
36 NK cells in secondary lymphoid organs from chronically SIVagm-infected AGM were frequently
37 CXCR5⁺ and entered and persisted in lymph node follicles throughout the follow-up (240 days
38 post-infection). These follicles were strongly positive for IL-15, which was primarily presented in
39 its membrane-bound form by follicular dendritic cells. Anti-IL-15-induced NK cell-depletion
40 during chronic SIVagm infection resulted in high viral replication (follicles and T zone) and viral
41 DNA increase in lymph nodes. Our data reveal that in non-pathogenic SIV infection, NK cells
42 migrate into follicles and play a major role for viral reservoir control in lymph nodes.

43

44

45 The persistence of Human immunodeficiency virus (HIV) in individuals treated efficiently with
46 combined antiretroviral therapy (cART) remains a tremendous obstacle to achieving sustained
47 virologic remission in HIV-infected individuals¹. A major anatomical HIV reservoir are lymph
48 nodes (LN)^{2,3}. Studies in the non-human primate model for HIV, macaques (MAC) infected by
49 SIVmac, showed that during the first weeks post-infection (p.i.), the virus replicates solely in the
50 T cell zone of LNs⁴. Only later on the virus spreads to B cell follicles, where it replicates to a
51 large extent in follicular helper T cells (T_{FH})⁵⁻⁹. Moreover, numerous viral particles are trapped by
52 follicular dendritic cells (FDC) and remain infectious¹⁰. Finally, in chronic infection, more virus
53 is present in follicles than in the T zone^{11,12}. In HIV controllers, the virus also persists
54 preferentially in these LN follicles and productive infection is markedly restricted to T_{FH} cells¹³.
55 Follicles thus seem to constitute 'sanctuaries' for persistent viral replication even in HIV
56 controllers who are capable of developing potent anti-viral CD8⁺ T cell responses¹³. Indeed, B
57 cell follicles are mostly devoid of CD8⁺ T cells except for the rare follicular cytotoxic T cells¹⁴. In
58 patients under long-term cART, T_{FH} cells equally represent the major viral reservoir, potentially
59 complicating efforts to cure HIV infection with T cell immunotherapy^{15,16}.

60 NK cells play an essential role in viral infections^{17,18}. Little attention has however been given to
61 them in LN as their frequency is low in these tissues in contrast to other body compartments, such
62 as liver or uterus¹⁹. In rodent LN, NK cells are more dense in the medulla than in T or B cell areas
63 and they are mainly located within lymphatic sinuses^{20,21}. Upon immunization or viral challenge
64 in rodents, NK cells infiltrate draining LNs^{22,23}. Little information is available regarding the
65 trafficking of NK cells to LN during viral infections in humans and on NK cell migratory
66 behavior within LN in general. During HIV-1 or SIVmac infections, LN display limited
67 recruitment of NK cells that instead seems to be deviated toward the intestinal mucosa, and
68 therefore provide a niche where the virus can replicate unabated by early NK-cell-mediated innate
69 pressure^{24,25}.

70 Non-human primates from Africa, such as African Green monkeys (AGM), are natural hosts of
71 SIV²⁵. They usually do not experience disease progression, despite displaying high viremia and

high viral replication in the intestine concomitant with massive acute depletion of mucosal CD4⁺ T cells²⁶. A major distinction of SIV infection in natural hosts is the rapid resolution of viral inflammation and the lack of microbial translocation^{3,25}. In addition, AGM display a rapid control of viral replication in the secondary lymphoid organs and lack of viral trapping by FDC in follicles²⁷⁻³³. Another natural host of SIV, the sooty mangabey, also showed strong viral control in LN^{6,34}.

In AGM, most pro-inflammatory cytokines such as TNF- α , IL-6, IFN- γ and IL-8 are not or only weakly induced upon SIV infection²⁵. However, AGM display high plasma levels of IFN- γ and IL-15 during acute infection³⁵. IL-15 is well known to promote mobilization and homeostatic proliferation of T cells and to be essential for the survival of NK cells^{36,37}. Moreover, IL-15 contributes to the preservation of cytotoxic CD8⁺T cells and also enhances NK cell suppressor function³⁸. We have observed increases in NK cell proliferation as well as of CD107a⁺ NK cells in peripheral LN during acute SIVagm infection³⁵. We therefore raised the question whether NK cells play a role during non-pathogenic SIV infection in LN. Here we demonstrate that NK cells accumulate in a CXCR5- and IL-15-dependent manner in follicles of secondary lymphoid organs in SIV-infected AGM and exert efficient control of viral replication within LN contributing to a low viral reservoir in these organs.

RESULTS

Lack of virus in lymph node follicles during non-pathogenic SIV infection

We first determined the level and distribution of virus in LN of six AGM and six MAC infected with SIVagm.sab92018 and SIVmac251, respectively. Plasma viral RNA copies were always at least as high in AGM as in MAC (Supplementary Fig.1a-c). The viremia peak was reached around day 9 p.i. for all animals. The quantification of the cell-associated (ca) viral RNA and ca-viral DNA copy numbers in LN cells showed similar high levels for both SIVagm and SIVmac infections at peak viremia (Fig.1a and Supplementary Fig.1d). However, a strong decrease was observed after the viral peak in AGM LN (p=0.001). This viral control in AGM LN resulted in a strong difference compared to SIVmac infection, as the median quantity of ca-viral RNA and

DNA in LN were, respectively, 2.5 log and 1.5 log lower in AGM than MAC during the chronic phase (Fig.1a and Supplementary Fig.1d). *In situ* evaluation of viral RNA showed indeed a dramatic decrease of productively infected cells in the T zone of AGM LN during the chronic phase of infection and a constant absence of productively infected cells within the follicles of AGM throughout the follow-up (240 days p.i.) (Fig.1b,c). These results contrast with SIVmac infection where, as expected, large amounts of viral RNA were detected both in the T zone and within follicles during chronic infection throughout the follow-up (Fig.1b,c).

Accumulation of NK cells in lymph node follicles during non-pathogenic SIV infection

NK cells were gated as previously reported (Supplementary Fig.2)^{35,39}. A progressive and persistent reduction in the frequency of LN NK cells was observed during chronic infection as compared to pre-infection levels in the pathogenic model ($p<0.001$), but not in AGMs where, after a transient decline, NK cells recovered to pre-infection levels ($p=0.8$) (Fig.1d). The decrease in MAC was due to a decline of the major NK cell population in LN (i.e. CD16⁻ NK cells), while, as in a previous report in macaque LN³⁹, there was an increase in CD16⁺ NK cells in SIVmac infection ($p<0.001$) (Fig.1g).

Evaluation of NK cell distribution *in situ* showed that in uninfected animals, NK cells were localized as expected in the marginal and parafollicular zone in both species (Supplementary Fig.3a). The localization of NK cells however changed dramatically in response to SIV infection. Indeed, many NK cells were found outside the marginal zones following SIV infection in both species (Supplementary Fig.3b+c). Of note, the distribution became highly distinct between pathogenic and non-pathogenic SIV infection. In SIV-infected AGM, NK cells were mostly found around or within follicles (Fig.1e,f and Supplementary Fig.3b), whereas MAC NK cells followed a random distribution within the LN after SIV infection and did not accumulate in follicles (Fig.1e,f and Supplementary Fig.3c). The total numbers of NK cells decreased in the T cell zone in both species after SIV infection. In contrast, NK cell numbers increased in follicles of AGM (Fig.1h).

These analyses reveal that NK cell distribution within LN changes significantly in response to SIV infection and differently between pathogenic and non-pathogenic infections. Moreover, the study in the non-pathogenic SIV infection uncovers that NK cells are able to migrate into follicles.

Decreases in LN homing receptors on NK cells in both pathogenic and non-pathogenic SIV infection

Since MAC showed persistently decreased NK cell levels in contrast to AGM, we wondered whether AGM NK cells have a better LN homing capacity than MAC during SIV infection. We examined the expression of major LN homing markers for NK cells (CCR7, CD62L, CX3CR1 and CXCR3). No significant changes as compared to pre-infection levels were detected on total peripheral blood NK cells for both species (Supplementary Fig.4a+b), while CD16⁻ NK cells displayed decreases in CXCR3 and CX3CR1 (Supplementary Fig.5a+b).

In LN, the frequencies of NK cells expressing CCR7, CD62L or CX3CR1 were markedly down-regulated in both pathogenic and non-pathogenic SIV infections (Supplementary Fig.4). The decreases were again more pronounced in the CD16⁻ than in the CD16⁺ subsets (Supplementary Fig.5).

Altogether, strong decreases of homing receptors were observed for both species, in particular for CD16⁻ NK cells. The homing receptor profiles were in most tissues similar between AGM and MAC and do not clearly explain the differences in NK cell levels in LN between AGM and MAC.

AGM NK cells express CXCR5 in secondary lymphoid organs during SIV infection

The preferential localization of NK cells in follicles during non-pathogenic SIV infection could be due to specific trafficking towards follicles and/or to an enhanced survival inside the follicles. In order to address the hypothesis of specific trafficking, we measured the expression of CXCR5 on NK cells. CXCR5 is known to be both necessary and sufficient for B and T_{FH} cell migration into follicles^{40,41}. We compared the level of CXCR5 expression on B cells, CD8⁺ T cells and NK

cells of LN from chronically infected animals (Fig.2a). As expected, the majority and minority of B and CD8⁺T cells, respectively, expressed CXCR5 (Fig.2a,b). The frequencies of CXCR5⁺NK cells were also low for MAC NK cells but, surprisingly, were elevated in AGM (Fig.2a,b). In contrast to spleen and LN, the levels of CXCR5⁺NK cells were similarly low in AGM and MAC in blood and gut (jejunum, colon) (Fig.2b).

Thus we have identified high levels of CXCR5⁺NK cells in LN of SIVagm-infected AGM. CXCR5 expression on AGM NK cells most likely allows their access to lymphoid tissue follicles.

Elevated frequencies of CD107a⁺ and CD32⁺CXCR5⁺NK cells in secondary lymphoid organs during non-pathogenic SIVagm infection

We wondered whether these CXCR5⁺NK cells could exert a suppressor function and characterized their functional phenotype. Major differences were observed between CXCR5⁺ and CXCR5⁻ NK cells in LN from SIV-infected AGM. Indeed CXCR5⁺NK cells expressed more frequently CD69, CD16, CD107a and the Fcγ receptor CD32 and more rarely NKG2D and NKp46 (Fig.2 c,d). These cells might thus possess both an ADCC as well as cytotoxic activity. The majority of CXCR5⁺NK cells (median 60%) were CD16⁺ (*not shown*). CXCR5⁺ NK cells were also more often PD-1⁺ than CXCR5⁻ NK cells (Fig.2d), which might be associated with their location in follicles.

We wondered whether these results are representative of other secondary lymphoid organs and analyzed spleen NK cells from 10 AGM and 10 MAC in chronic infection (Fig.3). First we quantified the ca-viral RNA and DNA loads in spleen. As in LN, they were significantly lower in AGM than in MAC (Fig.3a). The viral DNA levels were negatively correlated with NK cell levels in AGM but not in MAC (Fig.3c). As in LN, NK cell frequencies in spleen were higher in SIVagm than in SIVmac infection (Fig.3d). The frequency of CXCR5⁺NK cells in spleen was again significantly higher in AGM than in MAC, while the CXCR5⁺CD8⁺T cell frequencies were similar between the two species (Fig.3b,e). The major phenotypic difference between spleen CXCR5⁺NK and CXCR5⁻NK cells consisted in the higher levels of cells positive for CD107A⁺ and

CD32⁺ (Fig.3f). Also similar to LN, spleen CXCR5⁺NK cells were more often PD-1⁺ and less often NKp46⁺.

We then compared the NK cell phenotypes between AGM and MAC in LN and spleen. Since CXCR5⁺NK cells are rare in MAC, we compared total NK cells consisting in the majority of CXCR5⁺NK cells. No significant differences in the phenotype of these cells were observed between AGM and MAC, except that total NK cells from AGM in spleen were more frequently CD32⁺ than in MAC but the difference was weaker than for CXCR5⁺NK cells and was not observed in LN (Fig.2e and Fig.3g).

Altogether, we observed elevated levels of CXCR5⁺NK cells expressing CD32⁺ and CD107a⁺ in secondary lymphoid organs from SIVagm-infected AGM.

Follicles of AGM lymph nodes constitute a niche for trans-presentation of IL-15

Since NK cell numbers increased in follicles during SIVagm infection without clearly showing a better homing receptor expression profile than in macaques, we wondered whether additional mechanisms, such as *in situ* proliferation or increased survival, participate in the accumulation of NK cells in follicles during SIVagm infection. The levels of NK cell proliferation in LN, as measured by Ki-67 staining, were not higher during SIVagm than SIVmac infection (*not shown*). Because IL-15 is essential for NK cell survival, we studied IL-15 production and distribution in LN in response to SIV infection. We detected IL-15 in LN during both infections, but IL-15 production was significantly higher in chronically infected AGM than MAC (Fig.4a,b and Supplementary Fig.6). In addition, it was primarily limited to follicles, whereas in MAC the production was diffuse (Fig.4b and Supplementary Fig.6). Remarkably, we observed NK cells in AGM follicles most often only if the follicles were IL-15 positive (Fig.4d).

To identify the cellular source of IL-15 in the follicles, we examined the *ex vivo* expression of IL-15 in distinct hematopoietic and stromal cell subpopulations from the LN of infected animals. The gating was performed in such a way as to allow the identification of as many as seven distinct cell populations (Supplementary Fig.7a). We did not detect significant IL-15 production by intracellular staining even if the cells were stimulated with PMA/Ionomycin (*data not shown*).

Since intracellular detection of cytokines by flow cytometry was probably not sensitive enough, we evaluated *IL-15* mRNA *in situ* expression by FISH. Expression of *IL-15* mRNA was higher in AGM than in MAC LN (Fig.4e). Moreover, *IL-15* mRNA was expressed predominantly within follicles during SIVagm infection. Many mRNA-positive cells had dendritic-like shape and might thus correspond to FDC and/or dendritic cells located within the follicles.

IL-15 is particularly potent for stimulating immune responses if presented membrane-bound. We therefore co-stained the hematopoietic and stromal cell subpopulations for IL-15 and IL-15R α surface expression (Supplementary Fig.7). Most of the cells that presented membrane-bound IL-15 (mbIL-15; i.e. IL-15⁺IL-15R α ⁺ cells) corresponded to APC-like cells (CD3⁻CD4⁺) and stromal cells, including follicular dendritic cells (FDC). The most pronounced difference in the levels of mbIL-15 between AGM and MAC was observed for FDC (Fig.4c).

We next addressed the question whether distinct levels of IL-15R α between AGM and MAC could explain these profiles. IL-15R α expression was measured on the same cell populations as above. The percentages of IL-15R α ⁺ cells were highest for FDC, while the mean intensities of expression were highest on APC-like cells (CD3⁻CD4⁺) and FDC (Supplementary Fig.7b,c). This was the case for both AGM and macaques. Thus the IL-15R α expression levels were not responsible for higher levels of mbIL-15 in AGM.

Altogether, NK cell accumulation in follicles during non-pathogenic SIVagm infection was associated with the presence of high levels of IL-15. IL-15 was produced within the follicles and presented membrane-bound, in particular on FDC.

Anti-IL15 treatment of SIVagm-infected AGM induces NK cell depletion

A major question is if NK cells in AGM LN have a crucial impact on viral load. We therefore aimed to deplete NK cells *in vivo* in AGM. While there is presently no antibody specific for NK cells in primates, it has been recently reported that anti-IL-15 treatment preferentially and dramatically depletes NK cells in MAC³⁶. We treated five chronically infected AGM with this anti-IL-15 mAb using the same doses as previously described for MAC for a short period (2 weeks) (Fig.5a).

Blood NK cells were rapidly depleted (Fig.5b,c). The nadir was observed in 3 animals at day 7 post-treatment and for the two others at day 14. The latter two animals had higher NK cells at baseline. The levels remained low until autopsy at day 42 post-treatment. In contrast, the percentages of total blood CD4⁺ T cells showed only a slight, transient increase (p=0.043) and the absolute CD4⁺ T cell counts did not show any significant changes (p=0.21) (Fig.5d). The transient increases of CD4⁺ T cells might be explained by strong proliferation at days 7 and 14 (Fig.5f). Blood CD8⁺ T cell counts displayed a decrease that was mostly due to depletion of effector memory T cells (Fig.5e).

Anti-IL-15 depleted NK cells in all analyzed tissues, i.e. in LN, spleen and gut (Fig.5b and Supplementary Fig.8). In contrast to NK cells, the CD4⁺ and CD8⁺ T cell frequencies in LN were not different between day 0 and day 42 post-treatment (Fig.5g,h), with two exceptions. The frequencies of central memory CD4⁺ and effector memory CD8⁺ T cells were decreased in LN at days 21 and 42 post-treatment (Fig.5i,k).

Altogether, we show that anti-IL15 treatment induces a marked depletion of NK cells in SIVagm infected AGM in blood and tissues, including LN.

NK cell depletion during SIVagm infection leads to high viral replication in lymph nodes

We quantified the viral load in the anti-IL-15 treated animals. The viremia levels significantly increased and reached a median plateau around 10^5 viral RNA copies/ml at day 14 post-treatment (Fig.6a). Notably, in LN, both the ca-viral RNA and DNA were significantly increased (Fig.6b). *In situ* hybridization at days 21 and 42 post-treatment revealed many viral RNA-positive cells in LN of all treated animals (Fig.6c) and large foci of viral RNA-positive cells were detected in the T zone and within follicles. The increase in viremia in the blood of the anti-IL-15 treated animals is most likely the result of this increase in viral replication in the lymph nodes. There was no statistically significant correlation between the cell-associated vRNA or vDNA levels in LN and the proliferation (Ki-67) of total, naïve or or naïve, memory or effector CD8⁺ T cells in LN. This is the first time that a high number of SIV-infected cells are observed within follicles of AGM.

DISCUSSION

We present here the first documented evidence for a distinct anatomical location of NK cells in response to a lentiviral infection within LN in any species. Previous studies in mice have shown, that infections by *L. major* induce NK cells to be recruited to the paracortex²⁰. Similarly, we show that NK cells are recruited to the paracortex in response to SIV infection, but in addition we demonstrate here that NK cells can also accumulate around and within follicles of peripheral LNs in SIV-infected AGMs. This is an important observation, because it suggests the potential of NK cells to interact directly with other cells present in LN follicles, such as B cells and T_{FH} cells. It has been shown in murine models that NK cells can influence T_{FH} and germinal center B-cell responses⁴²⁻⁴⁵. Our results highlight the need for further studies on the effects of viral infections and vaccination on NK cell-B cell interactions and antibody responses, and on the potential role of NK cell localization within follicles in mediating these responses.

In contrast to B and T cells, the mechanisms governing NK cell trafficking remain poorly dissected. In this study, we correlated the capacity of NK cells to migrate into the follicles with CXCR5 expression. Moreover we show that IL-15, a NK survival molecule, was found at high

levels in follicles of SIVagm-infected AGM. IL-15 expression has been recently reported in LN of HIV-infected individuals, but only in the T zone⁴⁶. We have shown that IL-15 is produced within follicles and presented as membrane-bound in particular by FDC, but also by APC-like cells during SIVagm infection. This finding agrees with previous reports showing that human APC and FDC can present mbIL-15^{47,48}. The IL-15-mediated promotion of NK cell survival would then result in the accumulation of these cells in a critical region of the LN. These results support previous reports suggesting the existence of *in situ* differentiated NK cells in LN^{39,49}. The effect of IL-15 on NK cell survival, differentiation and function is much stronger when presented *in trans*, as it is the case here, than in its soluble form^{50,51}. *In vitro* studies have indeed shown that the decreased control of HIV-1 infection in CD4⁺ T cells by NK cells is due, at least *in vitro*, to the decreased presentation of mbIL-15⁴⁷. IL-15 induces LFA-1 expression which is a late step required for cytotoxic differentiation⁵². Thus, in addition to promoting NK cell survival, the IL-15 in the AGM follicles might contribute to the differentiation toward a mature cytotoxic phenotype⁵³. The study reveals that most of the CXCR5⁺ NK cells were indeed within the CD16⁺ subset and many expressed CD107a. In addition, the phenotypic analyses demonstrated that even more CXCR5⁺ NK cells expressed the Fc γ receptors CD16 and CD32. These NK cells might thus display superior antibody-dependent cellular cytotoxicity (ADCC). This needs to be confirmed by functional studies. Altogether, CXCR5⁺NK cells clearly showed a distinct phenotype that could explain their superior capacity for viral control.

We confirm here a strong viral control in LN during SIVagm infection. We cannot exclude that only follicles from peripheral secondary lymphoid organs are virus-free. It is still possible that lymphoid structures from the gut show viral replication and/or trapping since viral replication is not controlled in the gut in natural hosts. We also cannot exclude that in AGM the viral control in LN is stronger than in other natural hosts such as sooty mangabeys. However, our data are in line with previous reports on a strong SIVsm control in both the LN T zone and follicles of sooty mangabeys^{6,34}. HIV infection in LN causes inflammation that when untreated leads to collagen deposition, fibrosis and disruption of the LN architecture¹⁰. In addition, persistent HIV infection in LN might severely impact the development of effective immune cells^{54,55}. Our results highlight

that AGM have the extraordinary capacity to mount a tissue-specific viral control. Together with

other studies showing that memory CD4⁺T cells are less infected in natural hosts³, our data suggest that natural hosts, while unable to control viremia, developed mechanisms to specifically protect those key organs and cells which are critical for the education and memory of immune responses and protect secondary lymphoid structures from viral-induced damages. In addition, strong control of viral replication in the secondary lymphoid organs might contribute to the lack of inflammation during chronic infection in natural hosts.

NK cell depletion during SIVagm infection was associated with strong increases of viral replication in LN. This confirms the key role of NK cells for viral control in LN. The increase of viral replication was observed both in the T zone and within follicles. It is unclear which NK cell phenotype is associated with viral control in the T zone. It is possible that in AGM, NK cells are not exhausted in contrast to MAC, since AGM are capable to resolve chronic inflammation^{25,39}. We also cannot totally exclude that in the IL-15 treated animals, increases of CD4⁺ target cells or decreases of CD8⁺ T effector cells or their function contributed to the increases in viral load. However, in LN, the memory CD4⁺T cells were either decreased or unchanged. Regarding CD8⁺T cells, previous studies have shown that AGMs infected by SIVagm do not exhibit strong suppressive CD8⁺T cell capacities nor significant infiltrations of CD8⁺T cells into LN follicles^{28,56,57}. In addition, *in vivo* depletion of CD8⁺T cells in SIVagm-infected AGM have not lead to strong increases in viral load^{58,59}. It is still possible that CD8⁺T cells contribute to the control of viral load in the LN during SIVagm infection, but it is unlikely that they play a major role in this model.

Genetic and functional studies have long highlighted that NK cells impact significantly HIV infection¹⁸. However, the role of NK cells in the control of HIV/SIV reservoirs might have been underestimated in the past. NK cells play an important role for immune-surveillance in cancer. Clinical trials testing approaches for enhancing NK cell expansion and suppressor activity during cancer therapies are expanding. Based on our results, we anticipate that a better comprehension of NK cell biology in lymphoid tissues as provided here will endorse the search for novel NK-cell based immunotherapies in HIV infection.

Taken together, this study reveals that SIV infection induces a trafficking of NK cells within LNs. Most importantly, we discovered the potential of a unique, CXCR5⁺ and IL-15 dependent localization of NK cells within LN follicles. This study therefore uncovers a new feature of NK cells during viral infections. Furthermore, we provide here the evidence that NK cells during non-pathogenic SIVagm infection play an unforeseen key role in the control of viral replication in lymph nodes. The discovery that NK cells have the potential to efficiently control the viral reservoir in follicles might have important implications for cure and vaccine research.

METHODS

Methods are available online.

REFERENCES

1. Saez-Cirion, A., Jacquelin, B., Barré-Sinoussi, F. & Müller-Trutwin, M. Immune responses during spontaneous control of HIV and AIDS: what is the hope for a cure? *Philos. Trans. R. Soc. Lond. B. Biol. Sci.* **369**, 20130436 (2014).
2. Lederman, M. M. & Margolis, L. THE LYMPH NODE IN HIV PATHOGENESIS. *Semin. Immunol.* **20**, 187–195 (2008).
3. Paiardini, M. & Müller-Trutwin, M. HIV-associated chronic immune activation. *Immunol. Rev.* **254**, 78–101 (2013).
4. Chakrabarti, L. *et al.* Early stages of simian immunodeficiency virus infection in lymph nodes. *Amer J Pathol* **144**, 1226–1236 (1994).
5. Lindqvist, M. *et al.* Expansion of HIV-specific T follicular helper cells in chronic HIV infection. *J. Clin. Invest.* **122**, 3271–3280 (2012).

- 364 6. Brenchley, J. M. *et al.* Differential infection patterns of CD4+ T cells and lymphoid tissue viral
365 burden distinguish progressive and nonprogressive lentiviral infections. *Blood* **120**, 4172–
366 4181 (2012).
- 367 7. Petrovas, C. *et al.* CD4 T follicular helper cell dynamics during SIV infection. *J. Clin. Invest.*
368 **122**, 3281–3294 (2012).
- 369 8. Xu, H. *et al.* Persistent Simian Immunodeficiency Virus Infection Drives Differentiation,
370 Aberrant Accumulation, and Latent Infection of Germinal Center Follicular T Helper Cells. *J.*
371 *Virol.* **90**, 1578–1587 (2016).
- 372 9. Chowdhury, A. *et al.* Decreased T Follicular Regulatory Cell/T Follicular Helper Cell (TFH) in
373 Simian Immunodeficiency Virus-Infected Rhesus Macaques May Contribute to Accumulation
374 of TFH in Chronic Infection. *J. Immunol. Baltim. Md 1950* **195**, 3237–3247 (2015).
- 375 10. Estes, J. D. Pathobiology of HIV/SIV-associated changes in secondary lymphoid tissues.
376 *Immunol. Rev.* **254**, 65–77 (2013).
- 377 11. Tenner-Racz, K. & Racz, P. Follicular dendritic cells initiate and maintain infection of the
378 germinal centers by human immunodeficiency virus. *Curr. Top. Microbiol. Immunol.* **201**,
379 141–159 (1995).
- 380 12. Fox, C. H. *et al.* Lymphoid Germinal Centers Are Reservoirs of Human Immunodeficiency
381 Virus Type 1 RNA. *J. Infect. Dis.* **164**, 1051–1057 (1991).
- 382 13. Fukazawa, Y. *et al.* B cell follicle sanctuary permits persistent productive simian
383 immunodeficiency virus infection in elite controllers. *Nat. Med.* **21**, 132–139 (2015).
- 384 14. Leong, Y. A. *et al.* CXCR5(+) follicular cytotoxic T cells control viral infection in B cell follicles.
385 *Nat. Immunol.* (2016). doi:10.1038/ni.3543
- 386 15. Banga, R. *et al.* PD-1(+) and follicular helper T cells are responsible for persistent HIV-1
387 transcription in treated aviremic individuals. *Nat. Med.* (2016). doi:10.1038/nm.4113
- 388 16. Miles, B. & Connick, E. TFH in HIV Latency and as Sources of Replication-Competent Virus.
389 *Trends Microbiol.* **24**, 338–344 (2016).

- 390 17. Vivier, E., Tomasello, E., Baratin, M., Walzer, T. & Ugolini, S. Functions of natural killer cells.
391 *Nat. Immunol.* **9**, 503–510 (2008).
- 392 18. Carrington, M. & Alter, G. Innate immune control of HIV. *Cold Spring Harb. Perspect. Med.* **2**,
393 a007070 (2012).
- 394 19. Carrega, P. & Ferlazzo, G. Natural killer cell distribution and trafficking in human tissues.
395 *Front. Immunol.* **3**, (2012).
- 396 20. Bajénoff, M. *et al.* Natural killer cell behavior in lymph nodes revealed by static and real-
397 time imaging. *J. Exp. Med.* **203**, 619–631 (2006).
- 398 21. Garrod, K. R., Wei, S. H., Parker, I. & Cahalan, M. D. Natural killer cells actively patrol
399 peripheral lymph nodes forming stable conjugates to eliminate MHC-mismatched targets.
400 *Proc. Natl. Acad. Sci. U. S. A.* **104**, 12081–12086 (2007).
- 401 22. Beuneu, H. *et al.* Dynamic behavior of NK cells during activation in lymph nodes. *Blood* **114**,
402 3227–3234 (2009).
- 403 23. Sagoo, P. *et al.* In vivo imaging of inflammasome activation reveals a subcapsular
404 macrophage burst response that mobilizes innate and adaptive immunity. *Nat. Med.* **22**, 64–
405 71 (2016).
- 406 24. Luteijn, R. *et al.* Early viral replication in lymph nodes provides HIV with a means by which to
407 escape NK-cell-mediated control. *Eur. J. Immunol.* **41**, 2729–2740 (2011).
- 408 25. Huot, N., Rascle, P., Garcia-Tellez, T., Jacquelin, B. & Müller-Trutwin, M. Innate immune cell
409 responses in non pathogenic versus pathogenic SIV infections. *Curr. Opin. Virol.* **19**, 37–44
410 (2016).
- 411 26. Pandrea, I. V. *et al.* Acute loss of intestinal CD4⁺ T cells is not predictive of simian
412 immunodeficiency virus virulence. *J. Immunol. Baltim. Md 1950* **179**, 3035–3046 (2007).
- 413 27. Beer, B. *et al.* Lack of dichotomy between virus load of peripheral blood and lymph nodes
414 during long-term simian immunodeficiency virus infection of African green monkeys.
415 *Virology* **219**, 367–375 (1996).

- 416 28. Diop, O. M. *et al.* High levels of viral replication during primary simian immunodeficiency
417 virus SIVagm infection are rapidly and strongly controlled in African green monkeys. *J. Virol.*
418 **74**, 7538–7547 (2000).
- 419 29. Gueye, A. *et al.* Viral load in tissues during the early and chronic phase of non-pathogenic
420 SIVagm infection. *J. Med. Primatol.* **33**, 83–97 (2004).
- 421 30. Goldstein, S. *et al.* Wide range of viral load in healthy african green monkeys naturally
422 infected with simian immunodeficiency virus. *J Virol* **74**, 11744–53 (2000).
- 423 31. Broussard, S. R. *et al.* Simian immunodeficiency virus replicates to high levels in naturally
424 infected African green monkeys without inducing immunologic or neurologic disease. *J Virol*
425 **75**, 2262–75 (2001).
- 426 32. Cumont, M.-C. *et al.* Early divergence in lymphoid tissue apoptosis between pathogenic and
427 nonpathogenic simian immunodeficiency virus infections of nonhuman primates. *J. Virol.*
428 **82**, 1175–1184 (2008).
- 429 33. Müller, M. C. & Barré-Sinoussi, F. SIVagm: genetic and biological features associated with
430 replication. *Front. Biosci. J. Virtual Libr.* **8**, d1170-1185 (2003).
- 431 34. Martinot, A. J. *et al.* Acute SIV infection in sooty mangabey monkeys is characterized by
432 rapid virus clearance from lymph nodes and absence of productive infection in germinal
433 centers. *PloS One* **8**, e57785 (2013).
- 434 35. Jacquelin, B. *et al.* Innate immune responses and rapid control of inflammation in African
435 green monkeys treated or not with interferon-alpha during primary SIVagm infection. *PLoS*
436 *Pathog.* **10**, e1004241 (2014).
- 437 36. DeGottardi, M. Q. *et al.* Effect of Anti-IL-15 Administration on T Cell and NK Cell
438 Homeostasis in Rhesus Macaques. *J. Immunol. Baltim. Md 1950* **197**, 1183–1198 (2016).
- 439 37. Cooper, M. A. *et al.* In vivo evidence for a dependence on interleukin 15 for survival of
440 natural killer cells. *Blood* **100**, 3633–3638 (2002).

- 441 38. Li, J. *et al.* Differential effects of IL-15 on the generation, maintenance and cytotoxic
442 potential of adaptive cellular responses induced by DNA vaccination. *Vaccine* **33**, 1188–1196
443 (2015).
- 444 39. Schafer, J. L., Li, H., Evans, T. I., Estes, J. D. & Reeves, R. K. Accumulation of Cytotoxic CD16+
445 NK Cells in Simian Immunodeficiency Virus-Infected Lymph Nodes Associated with In Situ
446 Differentiation and Functional Anergy. *J. Virol.* **89**, 6887–6894 (2015).
- 447 40. Gunn, M. D. *et al.* A B-cell-homing chemokine made in lymphoid follicles activates Burkitt's
448 lymphoma receptor-1. *Nature* **391**, 799–803 (1998).
- 449 41. Moser, B., Schaerli, P. & Loetscher, P. CXCR5(+) T cells: follicular homing takes center stage
450 in T-helper-cell responses. *Trends Immunol.* **23**, 250–254 (2002).
- 451 42. Rydzynski, C. *et al.* Generation of cellular immune memory and B-cell immunity is impaired
452 by natural killer cells. *Nat. Commun.* **6**, 6375 (2015).
- 453 43. Abruzzo, L. V. & Rowley, D. A. Homeostasis of the antibody response: immunoregulation by
454 NK cells. *Science* **222**, 581–585 (1983).
- 455 44. Blanca, I. R., Bere, E. W., Young, H. A. & Ortaldo, J. R. Human B cell activation by autologous
456 NK cells is regulated by CD40-CD40 ligand interaction: role of memory B cells and CD5+ B
457 cells. *J. Immunol. Baltim. Md 1950* **167**, 6132–6139 (2001).
- 458 45. Yuan, D., Koh, C. Y. & Wilder, J. A. Interactions between B lymphocytes and NK cells. *FASEB*
459 *J. Off. Publ. Fed. Am. Soc. Exp. Biol.* **8**, 1012–1018 (1994).
- 460 46. Younes, S.-A. *et al.* IL-15 promotes activation and expansion of CD8+ T cells in HIV-1
461 infection. *J. Clin. Invest.* **126**, 2745–2756 (2016).
- 462 47. Moreno-Nieves, U. Y. *et al.* NK cells are primed by ANRS MVA(HIV)-infected DCs, via a
463 mechanism involving NKG2D and membrane-bound IL-15, to control HIV-1 infection in CD4+
464 T cells. *Eur. J. Immunol.* **44**, 2370–2379 (2014).

- 465 48. Park, C.-S., Yoon, S.-O., Armitage, R. J. & Choi, Y. S. Follicular Dendritic Cells Produce IL-15
466 That Enhances Germinal Center B Cell Proliferation in Membrane-Bound Form. *J. Immunol.*
467 **173**, 6676–6683 (2004).
- 468 49. Freud, A. G. *et al.* A human CD34(+) subset resides in lymph nodes and differentiates into
469 CD56bright natural killer cells. *Immunity* **22**, 295–304 (2005).
- 470 50. Stonier, S. W. & Schluns, K. S. Trans-presentation: a novel mechanism regulating IL-15
471 delivery and responses. *Immunol. Lett.* **127**, 85–92 (2010).
- 472 51. Tamzalit, F. *et al.* IL-15/IL-15R α complex shedding following trans-presentation is essential
473 for the survival of IL-15 responding NK and T cells. *Proc. Natl. Acad. Sci. U. S. A.* **111**, 8565–
474 8570 (2014).
- 475 52. Barao, I., Hudig, D. & Ascensao, J. L. IL-15-mediated induction of LFA-1 is a late step required
476 for cytotoxic differentiation of human NK cells from CD34+Lin- bone marrow cells. *J.*
477 *Immunol. Baltim. Md* **171**, 683–690 (2003).
- 478 53. Castillo, E. F., Stonier, S. W., Frasca, L. & Schluns, K. S. Dendritic cells support the in vivo
479 development and maintenance of NK cells via IL-15 trans-presentation. *J. Immunol. Baltim.*
480 *Md* **183**, 4948–4956 (2009).
- 481 54. Onabajo, O. O. & Mattapallil, J. J. Expansion or depletion of T follicular helper cells during
482 HIV infection: consequences for B cell responses. *Curr. HIV Res.* **11**, 595–600 (2013).
- 483 55. Racz, P., Tenner-Racz, K. & Schmidt, H. Follicular dendritic cells in HIV-induced
484 lymphadenopathy and AIDS. *APMIS. Suppl.* **8**, 16–23 (1989).
- 485 56. Zahn, R. C. *et al.* Simian immunodeficiency virus (SIV)-specific CD8+ T-cell responses in
486 vervet African green monkeys chronically infected with SIVagm. *J. Virol.* **82**, 11577–11588
487 (2008).
- 488 57. Lozano Reina, J.-M. *et al.* Gag p27-specific B- and T-cell responses in Simian
489 immunodeficiency virus SIVagm-infected African green monkeys. *J. Virol.* **83**, 2770–2777
490 (2009).

- 491 58. Schmitz, J. E. *et al.* Inhibition of adaptive immune responses leads to a fatal clinical outcome
492 in SIV-infected pigtailed macaques but not vervet African green monkeys. *PLoS Pathog.* **5**,
493 e1000691 (2009).
- 494 59. Gaufin, T. *et al.* Experimental depletion of CD8+ cells in acutely SIVagm-infected African
495 Green Monkeys results in increased viral replication. *Retrovirology* **7**, 42 (2010).
- 496 60. Jacquelin, B. *et al.* Nonpathogenic SIV infection of African green monkeys induces a strong
497 but rapidly controlled type I IFN response. *J. Clin. Invest.* **119**, 3544–3555 (2009).
- 498
- 499

ONLINE METHODS

Animals, SIV infections and anti-IL15 treatment

Fifteen African green monkeys (Caribbean *Chlorocebus aethiops*) and fifteen cynomolgus macaques (*Macaca fascicularis*) were used in this study. The animals were free of simian retrovirus type D and simian T-lymphotropic virus type 1 and were housed in single cages within level 3 biosafety facilities at the IDMIT Center (Fontenay-aux-Roses, France). Because H6 haplotypes are significantly associated with viral control in cynomolgus macaques, macaques with H6 haplotype were excluded from this study. The average weight of the monkeys was between 3 and 5 kg. All monkeys were young adults and with an average of 3 to 4 years at inclusion. Both males and females were used (60 % of females and 40 % of males for each species). The sample size varied between 5 and 10 animals per group (N=6 in most experiments), chosen according to the tripartite harmonized ICH Guideline on Methodology (previously coded Q2B). Sample collection was determined in a random order. The investigators were unblinded, while the animal handlers were blinded.

Animals were sedated with Ketamine Chlorhydrate (Rhone-Mérieux, Lyons, France) before handling. All experimental procedures were conducted in strict accordance with the international European guidelines 2010/63/UE on protection of animals use for experimentation and other scientific purposes (French decree 2013-118) and with the recommendations of the Weatherall report. IDMIT center complies with Standards for Human Care and Use of the Office for Laboratory Animal Welfare (OLAW, USA) under OLAW Assurance number #A5826-86. The monitoring of the animals was under the supervision of the veterinarians in charge of the animal facilities. Animal experimental protocols were approved by the Ethical Committee of Animal Experimentation (CETEA-DSV, IDF, France) (Notification #12-098). AGM and macaques were infected IV with, respectively, 250 TCID₅₀ of SIVagm.sab₉₂₀₁₈ and 5000 AID₅₀ of SIVmac₂₅₁, as previously reported^{28,35}.

From the six AGM and six MAC described in Figure 1, four of each species were randomly chosen for sacrifice at day 240 p.i., and the tissues (spleen and gut) collected at sacrifice used for

the analyses described in Figures 2 and 3. The spleens from the additional 6 animals described in Figure 3 correspond to randomly chosen, chronically SIVagm.sab92018-infected AGM from previous studies^{35,60}. The two remaining AGM from Figure 1 were included in the group of animals treated with the simianized anti-IL15 mAb. The three other AGMs treated with the anti-IL-15 mAb derived from previous studies and were also randomly chosen³⁵. The five AGMs were chronically infected with SIVagm.sab92018 for 1 to 3 years at the time of anti IL-15 administration.

Tissue collection and processing

Blood and LN biopsies were collected longitudinally. Whole venous blood was collected in EDTA tubes. Mononuclear cells were isolated by Ficoll density-gradient centrifugation. Biopsies of peripheral LNs were performed by excision. Other tissues (spleen, gut) were collected at autopsy. After careful removal of adhering connective and fat tissues, LN and spleen were digested using Collagenase IV, Collagenase D and DNase I and at 37°C for 5min. The tissue was then mechanically disrupted and filtered through a 40 µm cell strainer. Gut was washed with cold medium and cut in pieces. A 20 min digestion with Collagenase IV was performed at 37°C. The cell suspension was filtrated subsequently through 100 and 40 µm cell strainers and cells washed with cold PBS. Cells were either immediately stained for flow cytometry or cryopreserved in 90% FBS, 10% DMSO and stored in liquid nitrogen vapor.

Viral detection assays

Plasma viral load was determined by real-time PCR as described²⁸. For cell-associated viral RNA, RNA was extracted as follows: samples were lysed in NaCl (3M), EDTA (0.5M, pH 8), SDS (10%, Bio-Rad) and Proteinase K (1mg/mL, Qiagen) in a 45min incubation at 55° C. Then, NaCl (5M) was added and incubated at 4° C between 15 and 60min, followed by centrifugation for 15min at 3000rpm at 4° C. DNA was precipitated in Phenol:Chloroform:isoamyl alcohol 25:24:1 (pH = 8, Sigma Aldrich). Viral RNA was measured by qPCR in duplicate. SIVagm and SIVmac products of T7 transcription from plasmids were used as standards to calculate SIV RNA copy

numbers. 18SrRNA and CCR5 DNA quantification was used for normalization. Sample preparation, enzyme mix preparation and PCR set-up were performed in three separate rooms to avoid PCR contamination. Negative controls were used to exclude sample contamination.

Flow cytometry

All analyses on blood cells and most analyses on LN cells, including those on the homing receptors, were performed on fresh cells. Hypotonic ammonium chloride solution was used to lyse contaminating red blood cells. Cytofix/Cytoperm (BD Biosciences, La Jolla, CA) was used for all intracellular stainings. Intra cellular staining for IL-15 was performed without and after stimulation with Phorbol Myristate Acetate (PMA) and Ionomycin at final concentrations of respectively 10ng/mL and 1µg/mL. After 1 hour of incubation, 10 µg/mL of Brefeldin A was added. FcR blocking reagent (Miltenyi) was used to block unspecific antibody binding. Antibodies used are shown in Supplementary Table 1. Flow cytometry acquisitions were done on an LSR Fortessa (BD Biosciences), and FlowJo software (version 9.6.4, Tree Star, Ashland, OR) was used for all analyses.

Immunohistology

Fresh LN tissues were embedded and snap frozen in optimum cold temperature compound (OCT) and 10µm frozen sections were stained using unconjugated primary antibodies followed by appropriate secondary antibodies conjugated to Alexa 488 (green), Alexa 568 (red) (Molecular Probes, Eugene, OR). Antibodies used are shown in Supplementary Table 2. Stained slides were incubated with 100–200µL of ice cold methanol and 5% acetic acid, placed at -20°C for 10 min and then washed. Image analysis was performed using a Leica TCS SP8 confocal microscope equipped with white lasers (Leica Microsystems, Exton, PA).

Fluorescent *in situ* hybridization

The probes were prepared as follows. *SIVenv* and *IL-15* mRNA were RT-PCR amplified and cDNA was cloned, using the CloneJET PCR Cloning Kit (Thermo Fisher Scientific) as

recommended by the manufacturer. The vectors were digested and *in vitro* transcribed using T7 RNA polymerase (Ambion) to make Alexa Fluor 488 [Life Technologies] single-strand RNA probes. The FISH assay combined with immunofluorescent staining was performed as follows: Cryosections were rehydrated in PBS for 15 minutes and then permeabilized by incubating in 0.5% (v/v) Triton X-100 in PBS for 20 minutes at RT. The slides were placed in container filled with 200 ml of 10 mM sodium citrate buffer (pH 6.0) and the RNA unmasked by putting the container in a microwave set at 700 W, before heating for 2.5 minutes or until first signs of boiling. This step was repeated seven times. The slides were transferred to 2X SSC and subsequently incubated in formamide-SSC solution for at least 4 hours. The probe was mounted using glass chambers. Prehybridization was performed by incubating the slides with the mounted probe for 1-2 hours at 37°C. Cellular RNA and RNA probes were simultaneously denatured by incubating the slides with a mounted probe on a heating block for 5 minutes at 80°C, followed by hybridization in humid dark chambers for 1 day at 37°C. Sections were washed three times at high stringency in 0.1X SSC at 60°C and three times in 2X SSC buffer. Finally they were incubated in 0.05 µg/ml DAPI in SSC/Tween for 10 minutes, rinsed briefly in 2X SSC and mounted. As negative controls, we used a RNase degraded probe, as well as LNs from uninfected animals. Images were acquired on a Confocal Laser Scanning Microscope Leica TCS SP8, running LAS AF 3 (Leica Application Suite Advanced Fluorescence). Individual optical slices were collected at 1024 × 1024 pixel resolution. Image J software was used to assign colors to the channels collected.

Statistical analyses

Nonparametric Mann-Whitney *U*-tests was used to compare continuous factors between two groups, while non-parametric Wilcoxon signed rank test was used to compare paired variables. The Spearman rank correlation was used to assess the association between 2 continuous variables. These statistical analyses as well as graphic treatments were performed with GraphPad Prism 7.0 software (GraphPad Software, La Jolla, CA). To evaluate changes over time, mixed effect models were used to account for multiple repeated measurements, with testing of interactions between

time and species, time being considered as a categorical or continuous variable depending on the number of values. We first assessed if the marker's distribution was Gaussian; if not, a logarithmic transformation was used and tested if efficient. Secondly, a LOWESS (locally weighted scatterplot smoothing) curve was used to assess whether the marker's trajectory was linear. Finally, a mixed effect linear or piecewise-linear model was applied. Stata 13 (Stata Corp., College Station, TX, USA) was used for the analyses. In all analyses, p-values <0.05 were considered significant.

ACKNOWLEDGMENTS

This work was supported by the « Investissements d'Avenir » program managed by the National Agency of Research (ANR) under reference ANR-10-LABX-77, the ANRS and the l'OREAL foundation. The Infectious Disease Models and Innovative Therapies (IDMIT) center in Fontenay-aux-Roses, France, was funded by the French government "Investissements d'Avenir" program for infrastructures (PIA) under grant ANR-11-INBS-0008, the PIA grant ANR-10-EQPX-02-01 funding the FlowCyTech facility at IDMIT. RKR was supported by NIH grant RO1 DE026014. The anti-IL-15 mAb was a gift from the NIH Non-Human Primate Reagent Resource supported by AI126683 and OD010976. NH and MJP were recipients of post-doctoral fellowships from, respectively, the French Vaccine Research Institute (Créteil, France) and SIDACTION. PR and TGT received a PhD fellowship from, respectively, the University Paris Diderot, Sorbonne Paris Cité, and the Pasteur-Paris University PhD program supported by the Institut Carnot Pasteur Microbes et Santé. We are grateful to veterinarians and the staff of the IDMIT animal facility, in particular Vanessa Contreras, Benoit Delache, Jean-Marie Helies, Virgile Monnet, Julie Morin and Christophe Joubert for their excellent work. We thank Lamya Irbah, Thierry Kortulewski and Catherine Chapon for access to the stellar IDMIT imaging core facility as well as Christelle Cassan, Sabrina Guenounou and Antonio Cosma for access to the state-of-the art IDMIT Flowcytech core facility.

AUTHOR CONTRIBUTIONS

640 N.H. contributed to the project design, has set up methods and performed the experiments; N.D-
641 B. provided samples; N.H., B.J., T.G-T, P.R. and M.J.P. proceeded the samples; P.R. prepared the
642 anti-15 probe; N.H. and Y.M. performed the statistical analyses; N.H., B.J., R.K.R. and M.M-T.
643 analyzed and interpreted the data; B.J. has prepared the ethical protocols; N.H. and M.M-T. wrote
644 the manuscript. M.M-T. conceived the project and directed the research.

645

646

LEGENDS

Figure 1. Numbers and distribution of SIV RNA and NK cells in lymph nodes. Peripheral LNs from six AGM and six macaques infected by SIVagm and SIVmac, respectively, were analyzed. **(a)** Cell-associated viral RNA in total LN cells. **(b)** Representative confocal images of LN sections from chronically infected animals stained for CD20 (green), SIV RNA (red) and total nucleus (blue). Cells containing viral RNA were detected by *in-situ* hybridization. The picture represents the distribution of the productively-infected cells in LNs. One representative picture in the B and T zones is shown for each species. The time points analyzed in chronic phase corresponded to days 80, 150 and 250 days p.i. **(c)** The graph on the left shows the numbers of SIV RNA positive-cells per follicle. A total of 24 follicles were counted. The graph on the right shows the numbers of follicles positive for SIV RNA. A total of 8 LN sections per animal were counted. **(d)** Frequencies of NK cells among total CD45⁺ lymphocytes in LNs of AGM (purple) and MAC (grey). **(e)** Percentages of follicles positive for at least one NK cell. A total of 32 LN sections were counted. **(f)** Examples of the distribution of NK cells in LNs during chronic SIVmac and SIVagm infections as evaluated by confocal imaging. NK cells were stained with anti-NKG2A (green) and B cells with anti-CD20 (purple). Staining of NK cells were verified with other markers, such as NKp30⁺ and NKp80⁺ (*not shown*). The analysis reveals the localization of NK cells in and around follicles during SIVagm infection in AGM. **(g)** Frequencies of CD16⁻ NK and CD16⁺ NK cells of LN in AGM (purple) and MAC (grey). **(h)** Numbers of NK cells in the T and B cell zones. A total of 32 LN sections from 6 animals per species were counted (4-6 sections per animal). A nonparametric Mann-Whitney *U*-tests, for panels c,e and h were applied. For panels d and g a mixed effect model was used. Asterisks indicate significant differences *p<0.05; **p<0.005; ***p<0.001. Median and inter-quartile range are shown. Dpi= days post-infection.

Figure 2. CXCR5 expression on NK cells and phenotyping of CXCR5⁺ NK cells in AGM.

CXCR5 was measured on cells from six chronically infected AGM and six chronically infected

macaques. **(a)** Gating strategy used to analyze CXCR5 expression on B cells, CD8⁺ T cells and NK cells. Cells from macaque are plotted in grey and from AGM in purple. Representative plots are shown. **(b)** Frequencies of CXCR5⁺ cells for a given cell population in LNs from distinct tissues. **(c)** Phenotype of CXCR5⁻ and CXCR5⁺ lymph node NK cells in AGM. A representative dot plot for one animal is shown. **(d)** Frequencies of CXCR5⁺ and CXCR5⁻ NK cells expressing a given marker in AGM LN. **(e)** NK cell subset frequencies in LN from AGM and MAC. Individual values for AGM are shown as purple circles and for MAC as grey squares. A nonparametric Mann-Whitney *U*-test, was applied **p*<0.05 ; ***p*<0.005; ****p*<0.001.

Figure 3. Viral load and NK cells in spleen from chronically infected AGM and MAC. Ten animals per species were analyzed. **(a)** Cell-associated SIV DNA and RNA in spleen **(b)** CXCR5⁺ NK cells. Representative dot plots for 5 out of 10 randomly chosen animals (alphabetic order) are shown. **(c)** Cell-associated viral DNA in spleen was plotted against the frequency of spleen NK cells of MAC (left) and AGM (right). **(d)** Frequencies of NK cells among CD45⁺ cells in spleen **(e)** Frequencies of CXCR5⁺ among NK and CD8⁺ T cells in spleen. **(f)** Frequencies of CXCR5⁺ and CXCR5⁻ NK cells expressing a given marker in spleen. **(g)** NK cell subsets in spleen from AGM and MAC. Individual values for AGM are shown as purple circles and of MAC as grey squares. In panel c a nonparametric Spearman's rank-order correlation was run to determine the relationship between LOG(DNAsiv) and NK cell frequencies for each species . For all panels except panel c, a nonparametric Mann-Whitney *U*-test, was applied **p* < 0.05; ***p*<0.005.

Figure 4. IL-15 expression in lymph nodes during SIV infection in AGM and macaques. LNs from six chronically infected AGM and six chronically infected macaques were analyzed. **(a)** Percentage of follicles positive for at least one IL-15⁺ cell per analyzed LN section. A total of 10 LN sections per animal were counted. **(b)** Confocal image of LN sections stained for IL-15 (red) and total nucleus (blue). The picture represents the distribution of IL-15 positive cells for

each species. IL-15 staining was strong in LNs from SIVagm-infected AGM and predominant in the follicles (c) Frequencies of cells positive for both IL-15 and IL-15R α among distinct cell subpopulations of stromal (CD45-) and hematopoietic (CD45+) cells. (d) Confocal image of LN sections stained for NK cells (green), IL-15 (red) and nucleus (blue), showing the spatial association between IL-15 and NK cells. The zooms on the right side show enlarged images of AGM follicles showing typical NK cell distribution in AGM follicles, i.e. within and surrounding IL-15 positive follicles during SIVagm infection (e) Confocal image of LN sections hybridized with a IL-15 RNA probe (red) and stained with DAPI (blue). IL-15 mRNA positive cells were mainly detected in follicles in both species. The enlargements display representative examples of the shape of the IL-15 mRNA positive cells. Nonparametric Mann-Whitney *U*-tests were applied. Asterisks indicate significant differences ($p < 0.05$). Median and interquartile range are shown. AGM : purple circle; MAC: grey squares. FDC= follicular dendritic cell.

Figure 5. Anti-IL-15 administration results in near-complete NK cell depletion in AGM. (a) Schematic representation of the anti-IL-15 treatment schedule used in this study. Five chronically infected AGM received 20 mg/kg of anti-IL-15 mAb on day 0 and 10 mg/kg on day 14. The red arrows show the days of anti-IL-15 mAb administration. The blue arrow indicates the day of necropsy (Nx). (b) Dot plots showing NK cells (CD3⁻NKG2A⁺) in peripheral blood of one representative AGM before and after anti-IL-15 administration (c) Follow up of NK cells in blood and LN. In blood, five animals were followed. LN were available for 4 and 5 animals LN at day 21 and d42 post-treatment, respectively. In blood, grey and purple lines represent the trajectories for each animal and the median values from all animals, respectively. For the statistical analyses, the mean values of the three pre-infection time points were used. (d) Follow up of CD4⁺T cells and CD4⁺T cell subpopulations in blood during anti-IL-15 treatment. (e) Follow up of CD8⁺T cells and CD8⁺T cell subpopulations in blood during anti-IL-15 treatment. (f) Levels of CD4⁺T and CD8⁺T positive for Ki-67 in blood. (g) CD4⁺T cells in LN (h) CD8⁺T cells in LN (i) CD4⁺T cell subpopulations in LN (k) CD8⁺T cell subpopulations in LN. Median values and interquartile range are indicated. Each dot represents the values of an individual

animal. T_N: naïve T cells; T_M: central memory T cells; T_E: Effector memory T cells.
Nonparametric Mann-Whitney *U*-tests were applied **p* < 0.05; ***p* < 0.005.

Figure 6. NK cell depletion results in increases of SIV RNA, SIV DNA and productively infected cells in lymph nodes. (a) Quantification of SIV_{agm.sab92018} RNA in plasma by qRT-PCR in 5 chronically infected AGM (the same as in Fig.5), before and after anti-IL-15 administration. The grey line represents the viremia levels in individual monkeys over time and the purple line represents the median viremia. The black arrows show the days of anti-IL-15 administration. (b) Quantification of the cell-associated SIV RNA and DNA in LN. The LN of 6 animals without treatment were compared to LN from 5 anti-IL-15 treated monkeys. Each dot represents an individual animal (c) Virus-producing cells (SIV RNA, red) in the LN of NK cell-depleted AGM. Representative images of an inguinal LN from five different animals. One image for each of the five anti-IL-15 treated animals is shown. Follicles are delineated by the dashed white lines. Images derived from mounted multiple confocal projected z-scans. Pictures were obtained using a Leica SP8 confocal microscope and processed with ImageJ software. Confocal images were collected with a 40X objective. Tx= anti-IL15 treatment. Nonparametric Mann-Whitney *U*-tests were applied **p* < 0.05; ***p* < 0.005.

Supplementary Figure 1: Viral load in peripheral blood and lymph nodes from AGM and macaques (a) Quantification of SIVmac RNA in plasma in six macaques. (b) Quantification of SIVagm RNA in plasma in six AGM. (c) Median (interquartile range) values of plasma viral RNA in the six AGM and six macaques (d) Median (interquartile range) values of ca-viral DNA load in peripheral LN of the six AGM and six macaques.

Supplementary Figure 2. Gating strategy for identifying NK cells within blood and lymph nodes from MAC and AGM. Dot plots represent the main steps of the gating strategy that was the same as reported for other NHP studies^{35,39}. NK cells were defined by morphology and as CD45⁺ CD20⁻ CD3⁻ CD4⁻ NKG2A⁺ CD8^{+/-}. NK cells from LN were CD8^{low/neg} in contrast to blood NK cells that were CD8⁺. NKG2A was identified as the most inclusive NK cell marker in both AGM and macaques, as previously reported^{35,39}.

Supplementary Figure 3. Localization of NK cells in lymph nodes. (a) SIV-naive animals. Representative LN tissue section from a SIV-naive macaque, stained with anti-NKG2A (pink) to label NK cells, DAPI (blue) to label nucleus and anti-ER-TR7 (green) to label stromal cells (reticular fibroblasts). The enlarged figure shows NK cells (pink) and high endothelial venules (green). NK cells were mostly located in the medulla and sometimes in the paracortex. The same distribution was observed for NK cells in LN from non-infected AGMs. (b) Localization of NK cells in lymph nodes of chronically SIVagm-infected African green monkeys. (i+ii) Representative LN tissue sections stained with anti NKG2A (white) to label NK cells and with DAPI (blue) to label nucleus of all cells. (i) Inguinal LN from animal SV083 (AGM) at day 150 p.i. (ii) Axillary LN from animal SV091 (AGM) at 150 day p.i. (iii) Magnification showing NK cells stained in green, B cells in white and nuclei in blue. Enlargements show examples of NK cells for both the B zone and T zone. NK cells were predominantly localized in the B zones (follicles), showing two types of predominant localization: most of the times they accumulated within follicles and sometimes they accumulated around the follicles (see also Fig.1f). (c) Localization of NK cells in lymph nodes of chronically SIVmac-infected macaques. (i+ii)

Representative LN tissue sections stained with anti NKG2A (white) to label NK cells and DAPI (blue) to label nucleus of all cells. (i) Inguinal LN section from animal CA275 (macaque) at day 150 p.i. (ii) Axillary LN section from animal CBB001 (macaque) at 150 days p.i. (iii) Magnifications showing B cells in white, NK cells in green and cell nuclei in blue. Starting from the acute phase, the distribution of NK cells in LN from SIV-infected macaques was different from that of non-infected animals. While in infected AGM and MAC, NK cells were found more often outside the medulla than in non-infected animals, NK cells in SIV-infected MAC were randomly distributed in the tissue and did not accumulate in follicles in contrast to SIVagm-infected AGM.

Supplementary Figure 4. Dynamics of lymph node homing markers on blood and lymph node NK cells in response to SIVmac and SIVagm infection. Blood and LN cells were analyzed, respectively, 3 times and one time before infection and 3 times during the chronic phase (days 80, 150, and 250 p.i.) (a) The levels of NK cells expressing homing markers were compared in the same animals before and in chronic infection. The values for the six AGM are depicted in green and for the six macaques in red. Statistically significant differences are indicated by asterisks (* $p < 0.05$; *** $p < 0.001$;). (b) The levels of NK cells expressing homing markers are shown before infection and longitudinally for each time point in chronic infection. The values for the six AGM are depicted in violet and for the six macaques in grey. Median and interquartile range are shown. Nonparametric Mann-Whitney *U*-tests were applied for each panel.

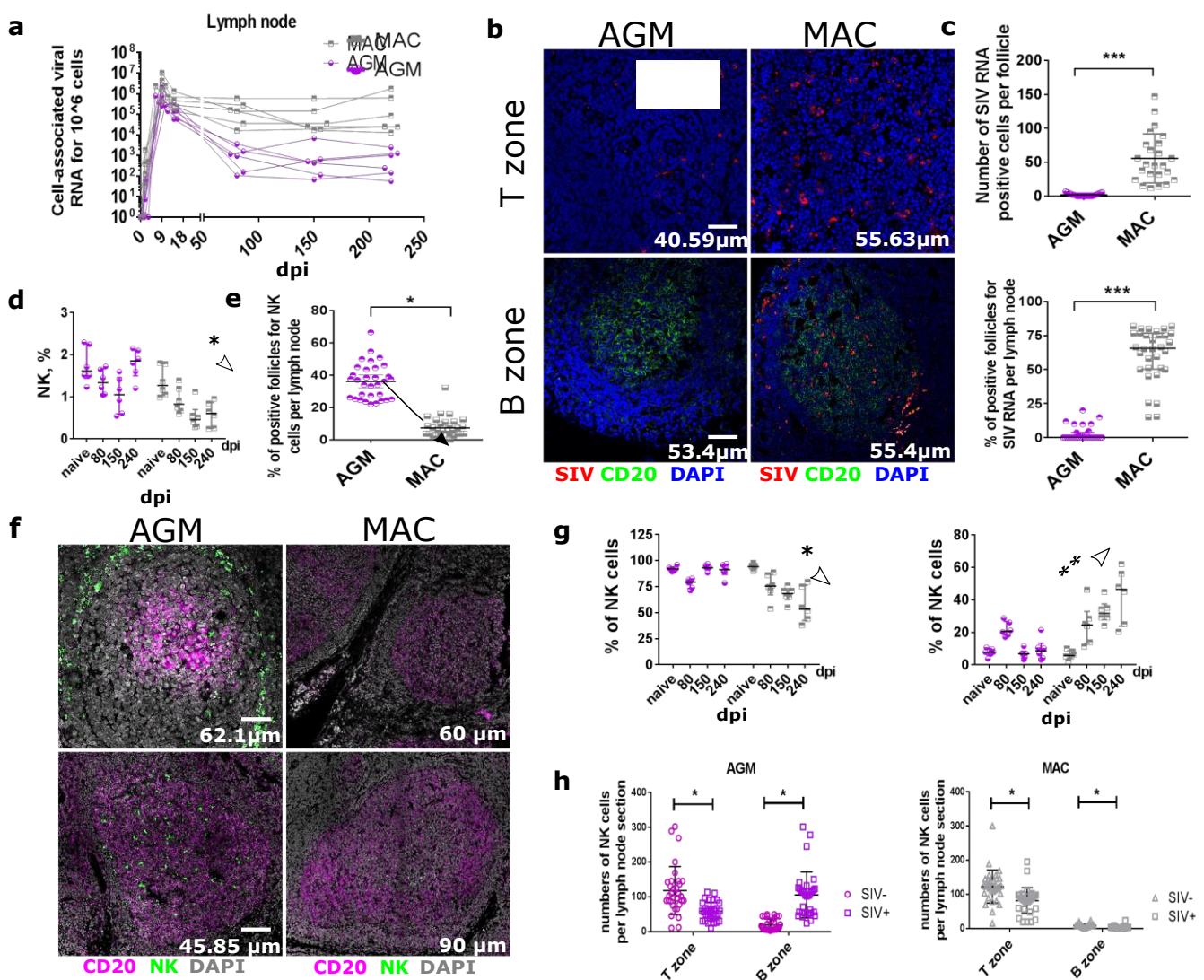
Supplementary Figure 5. Follow up of homing markers on CD16⁺ and CD16⁻ NK cells in blood and lymph nodes from AGM and MAC before and in chronic SIV infection. Blood and LN cells were analyzed, respectively, 3 times and one time before infection and 3 times during the chronic phase (days 80, 150, and 250 p.i.) from six AGM and six macaques (a). The levels of CD16⁺ and CD16⁻ NK cells expressing specific

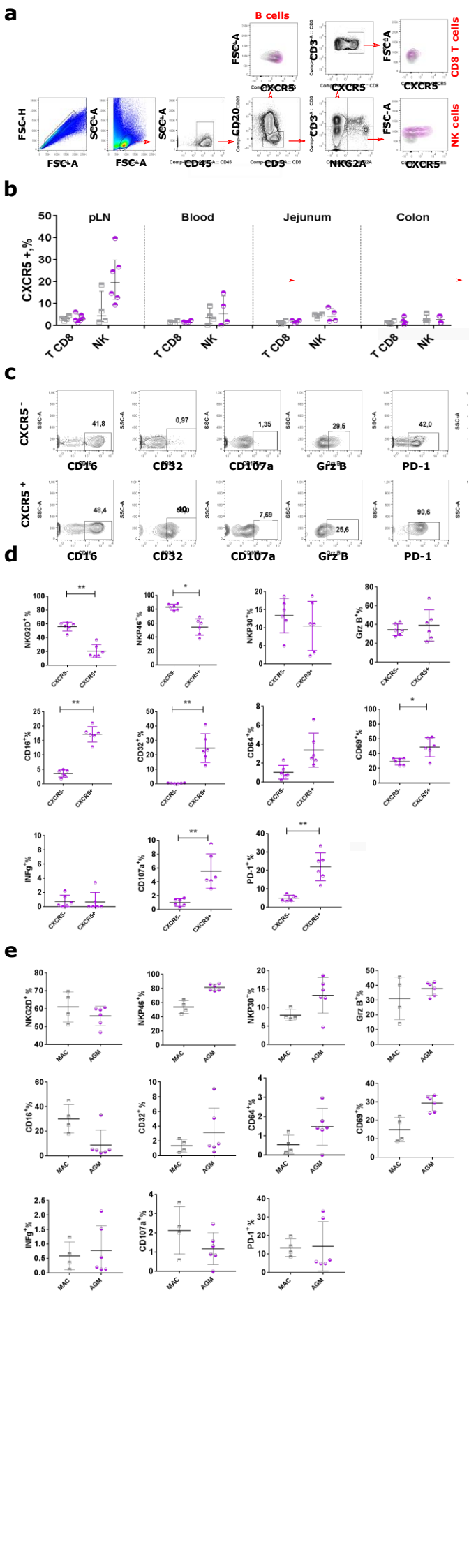
homing markers were compared in the same animals before and in chronic infection. **(b)** The levels of CD16⁺ and CD16⁻ NK cells expressing specific homing markers are shown before infection and for each time point in chronic infection. Nonparametric Mann-Whitney *U*-tests were applied. Statistically significant differences are indicated by asterisks (*** $p < 0.001$; * $p < 0.05$). Median and interquartile ranges are shown.

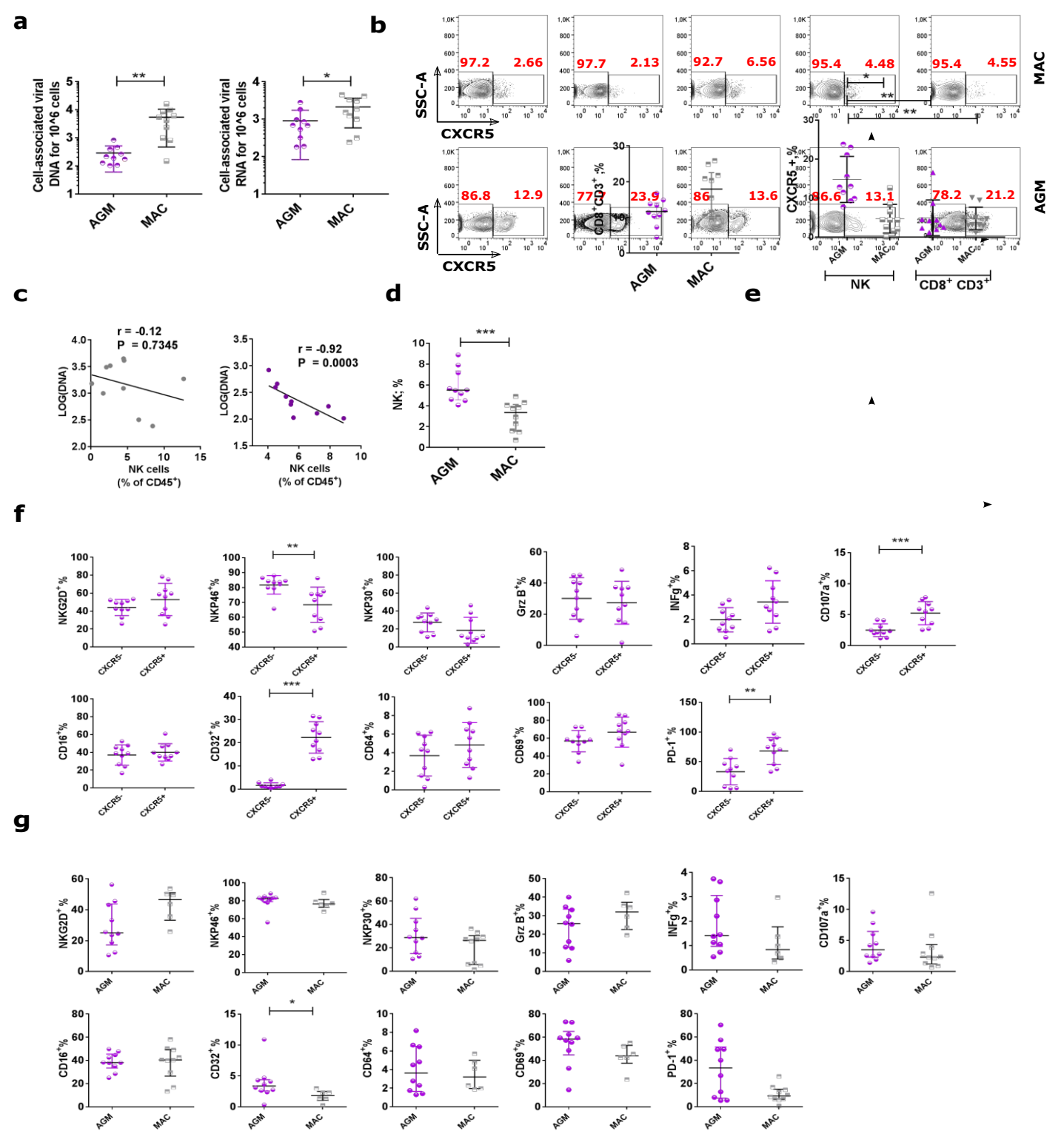
Supplementary Figure 6. IL-15 expression in lymph nodes from chronically SIV-infected AGM and macaques. Representative LN tissue sections stained with anti IL-15 (red), CD20 (white) and Dapi (blue). The first two rows at the top show inguinal and axillary LN sections from chronically infected AGM. The third row shows axillary LN section from a chronically infected macaque. More IL-15 staining was observed in AGM. In AGM, IL-15 positive cells were mainly present in follicles. In macaques, IL-15 was weak and IL-15-positive cells were distributed randomly in the LNs.

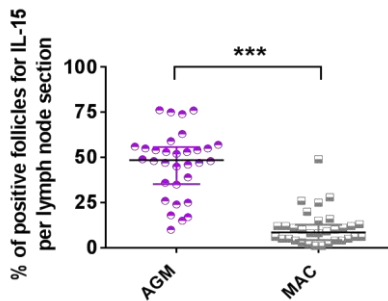
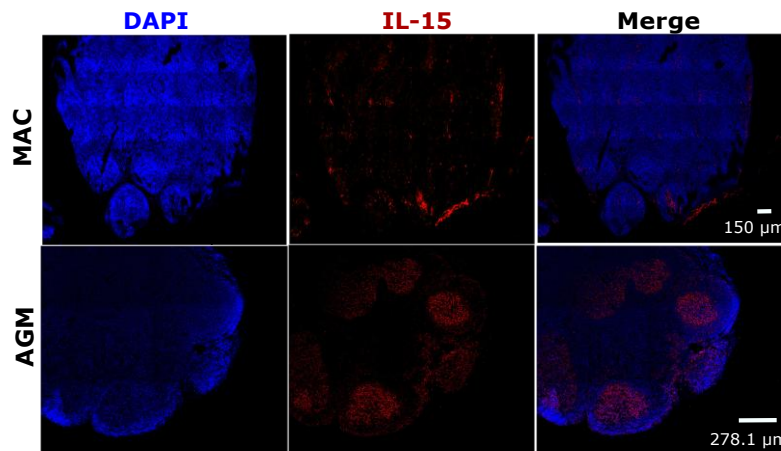
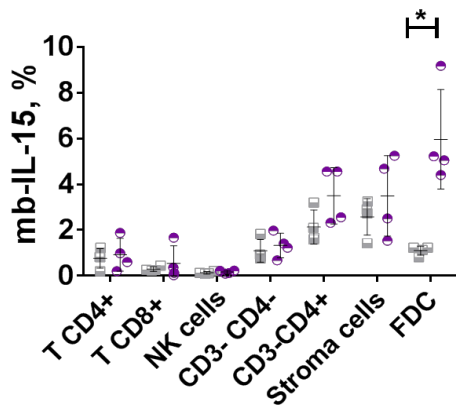
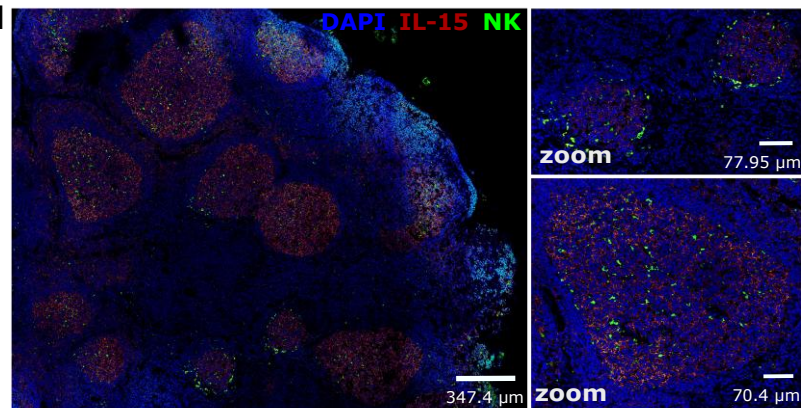
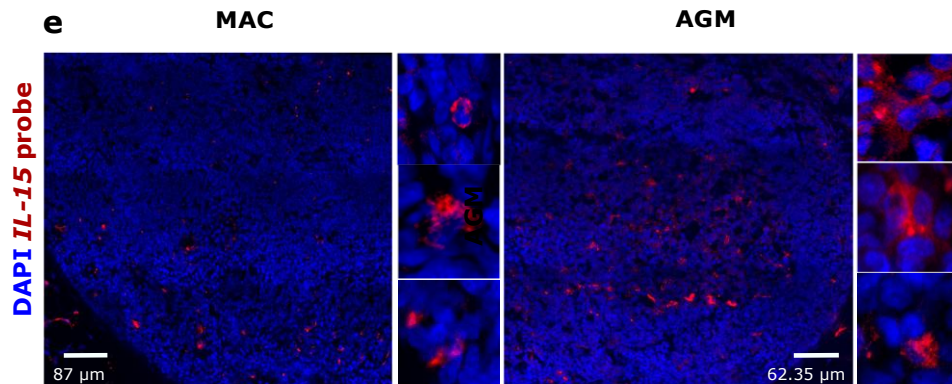
Supplementary Figure 7. Representative gating strategy for identifying membrane-bound IL-15 in total lymph node cells from chronically SIV-infected AGM and macaques. (a) Frozen LN cells from chronically SIV-infected animals were used for the analysis. Living cells were identified as Aqua dye-negative. LN cell sub-populations were defined as follows: stromal cells as CD45⁻ CD16⁻ Podoplanin⁻ ; FDC as CD45⁻ CD16⁺ Podoplanin⁺ ; CD4 T cells as CD45⁺ CD3⁺ CD4⁺ ; CD8 T cells as CD45⁺ CD3⁺ CD8⁺ ; NK cells as CD45⁺ CD3⁻ NKG2A⁺ ; and two other population as CD45⁺ CD3⁻ CD8⁻ CD16⁻ NKG2A⁻ CD4^{+/+}. Positive cells for mbIL-15 were defined when cells were double positive for IL-15 and IL-15R α . **(b)** Mean of fluorescent intensity of IL-15R α on the LN cell-subpopulations described above **(c)** Frequency of IL-15R α ⁺ cells in LN cell-subpopulations. Nonparametric Mann-Whitney *U*-tests were applied. Statistically significant differences are indicated by asterisks (*** $p < 0.001$; * $p < 0.05$). Median and interquartile ranges are shown.

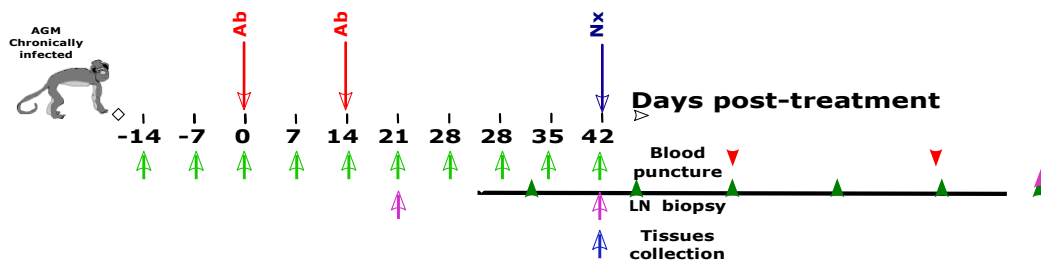
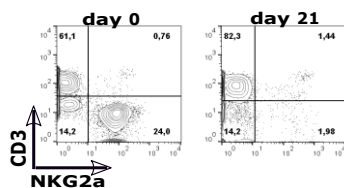
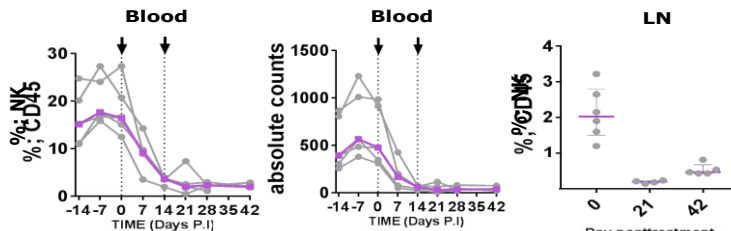
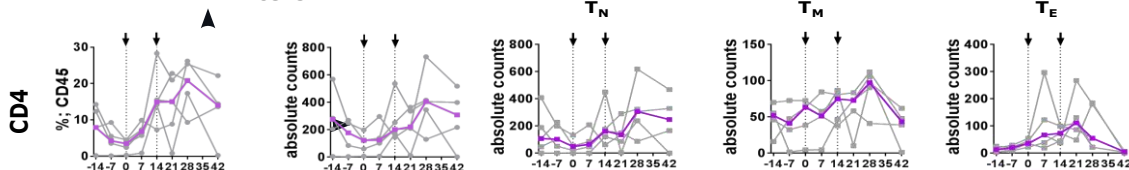
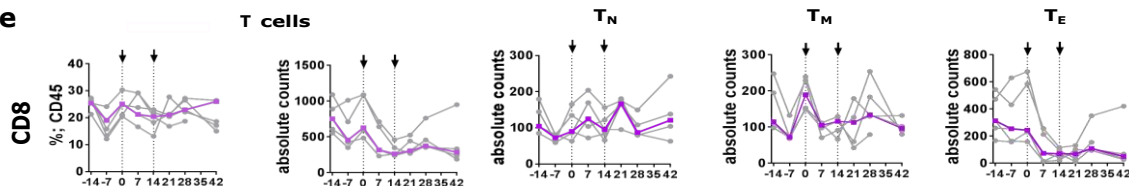
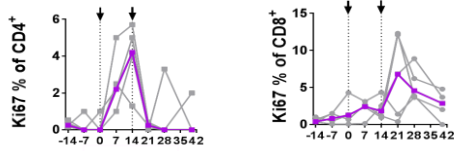
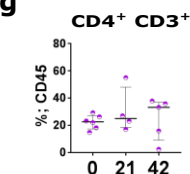
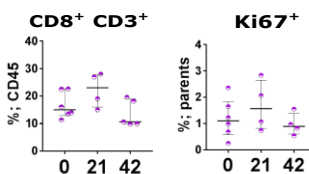
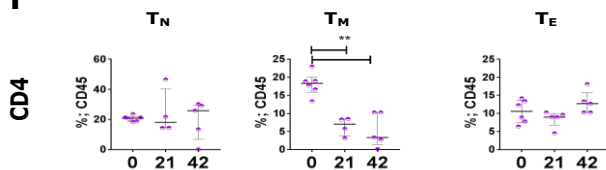
Supplementary Figure 8. Cell phenotypes and frequencies in chronically infected AGM treated with anti IL-15. (top) NK cell, T CD4 cell and T CD8 cell frequencies in tissues from chronically SIVagm-infected AGM without and after anti-IL-15 treatment. Tissues (spleen and four gut compartments) were obtained at necropsy. Samples from 4 non-treated (black circles) and five anti-IL-15 treated AGM (grey squares) were available for the analyses. NK cells were significantly depleted in duodenum, ileon, jejunum and spleen, while no significant changes were observed for CD4⁺ and CD8⁺ T cells in gut or spleen. **(middle)** Frequencies of each T cell subset within CD45⁺ cells in blood. Five AGMs were studied. Individual animals are depicted by grey lines and the purple line represents the median values. **(bottom)** Frequencies of Ki-67⁺ cells for each T cell subset at days 0, 21 and 42 post-treatment. LN from 4 AGM at day 21 and 5 animals at day 42 post-treatment were available. Each circle represents the value of an individual AGM. The black arrows indicate the days of anti-IL15 administration. T_N: naïve T cells; T_M: central memory T cells; T_E: effector memory T cells. Nonparametric Mann-Whitney *U*-tests were applied. Statistically significant differences are indicated by asterisks (***) $p < 0.001$; * $p < 0.05$). Median and interquartile ranges are shown.







a**b****c****d****e**

a**b****c****d****T cells****e****T cells****f****g****h****i****k**